

Anomalous valley Hall effect in two-dimensional valleytronic materials

Hongxin Chen(陈洪欣), Xiaobo Yuan(原晓波), and Junfeng Ren(任俊峰)

Citation: Chin. Phys. B, 2024, 33 (**4**): 047302. DOI: 10.1088/1674-1056/ad1c59
Journal homepage: http://cpb.iphy.ac.cn; http://iopscience.iop.org/cpb

What follows is a list of articles you may be interested in

Recent progress on valley polarization and valley-polarized topological states in two-dimensional materials

Fei Wang(王斐), Yaling Zhang(张亚玲), Wenjia Yang(杨文佳), Huisheng Zhang(张会生), and Xiaohong Xu(许小红)

Chin. Phys. B, 2024, 33 (**1**): 017306. DOI: 10.1088/1674-1056/ad0713

Perspectives of spin-valley locking devices

Lingling Tao(陶玲玲)

Chin. Phys. B, 2023, 32 (**10**): 107306. DOI: 10.1088/1674-1056/acc809

Single-layer intrinsic 2H-phase LuX_2 (X = Cl, Br, I) with large valley polarization and anomalous valley Hall effect

Chun-Sheng Hu(胡春生), Yun-Jing Wu(仵允京), Yuan-Shuo Liu(刘元硕), Shuai Fu(傅帅),Xiao-Ning Cui(崔晓宁), Yi-Hao Wang(王易昊), and Chang-Wen Zhang(张昌文)

Chin. Phys. B, 2023, 32 (**3**): 037306. DOI: 10.1088/1674-1056/ac89d6

Spin- and valley-polarized Goos-Hänchen-like shift in ferromagnetic mass graphene junction with circularly polarized light

Mei-Rong Liu(刘美荣), Zheng-Fang Liu(刘正方), Ruo-Long Zhang(张若龙), Xian-Bo Xiao(肖贤波), and Qing-Ping Wu(伍清萍)

Chin. Phys. B, 2023, 32 (**3**): 037301. DOI: 10.1088/1674-1056/ac89e2

Goos-Hänchen-like shift related to spin and valley polarization in ferromagnetic silicene

Mei-Rong Liu(刘美荣), Zheng-Fang Liu(刘正方), Ruo-Long Zhang(张若龙), Xian-Bo Xiao(肖贤波), and Qing-Ping Wu(伍清萍)

Chin. Phys. B, 2021, 30 (**10**): 107302. DOI: 10.1088/1674-1056/ac1e16

RAPID COMMUNICATION

Improving the electrical performances of InSe transistors by interface engineering

Tianjun Cao(曹天俊)[1], Song Hao(郝松)[2,†], Chenchen Wu(吴晨晨)[1], Chen Pan(潘晨)[2], Yudi Dai(戴玉崠)[1], Bin Cheng(程斌)[2], Shi-Jun Liang(梁世军)[1,‡], and Feng Miao(缪峰)[1,§]

[1] *Institute of Brain-Inspired Intelligence, National Laboratory of Solid State Microstructures, School of Physics, Collaborative Innovation Center of Advanced Microstructures, Nanjing University, Nanjing* 210093, *China*

[2] *Institute of Interdisciplinary Physical Sciences, School of Physics, Nanjing University of Science and Technology, Nanjing* 210014, *China*

(Received 12 December 2023; revised manuscript received 30 January 2024; accepted manuscript online 1 February 2024)

InSe has emerged as a promising candidate for next-generation electronics due to its predicted ultrahigh electrical performance. However, the efficacy of the InSe transistor in meeting application requirements is hindered due to its sensitivity to interfaces. In this study, we have achieved notable enhancement in the electrical performance of InSe transistors through interface engineering. We engineered an InSe/h-BN heterostructure, effectively suppressing dielectric layer-induced scattering. Additionally, we successfully established excellent metal–semiconductor contacts using graphene ribbons as a buffer layer. Through a methodical approach to interface engineering, our graphene/InSe/h-BN transistor demonstrates impressive on-state current, field-effect mobility, and on/off ratio at room temperature, reaching values as high as 1.1 mA/μm, 904 $cm^2 \cdot V^{-1} \cdot s^{-1}$, and $> 10^6$, respectively. Theoretical computations corroborate that the graphene/InSe heterostructure shows significant interlayer charge transfer and weak interlayer interaction, contributing to the enhanced performance of InSe transistors. This research offers a comprehensive strategy to elevate the electrical performance of InSe transistors, paving the way for their utilization in future electronic applications.

Keywords: two-dimensional materials, InSe, van der Waals heterostructure, electrical performances, charge density difference

PACS: 73.20.–r, 73.40.Ns **DOI:** 10.1088/1674-1056/ad24d7

1. Introduction

Two-dimensional (2D) materials with high electrical performances, including high carrier mobility, on/off current ratio, on current density, etc. are essential for the preparation of next-generation high-performance electronic devices. The emergence of graphene inspired the exploration of its applications in high-performance electronics owing to its atomically thin structure and many utmost properties.[1–3] In parallel with bandgap-opening engineering for graphene,[4,5] the discovery of novel two-dimensional (2D) semiconducting materials with intrinsically suitable bandgap has become one of the most fascinating research topics.[6,7] Among these, the carrier mobilities of 2D transition metal dichalcogenides (TMDCs) are usually below several hundred $cm^2 \cdot V^{-1} \cdot s^{-1}$ which makes them difficult to be applied to the integration of high-performance electronic devices.[8–11] Black phosphorus is difficult to stabilize under ambient conditions and to synthesize large-scale films although it possesses high carrier mobility.[12–15] Different from the aforementioned materials, InSe in the γ-rhombohedral phase is theoretically predicted to possess high room-temperature carrier mobility due to small effective mass and relative stability at ambient conditions, which are comparable to that of strained silicon.[16–19]

InSe has demonstrated intrinsic high-charge transport behaviors experimentally, manifesting intriguing physical phenomena. For instance, ballistic avalanche phenomena within nanoscale vertical InSe/black phosphorus vdW heterostructures have been revealed.[20] Moreover, recent studies illustrated the emergence of sliding ferroelectricity in γ-phase InSe induced by yttrium-doping and intrinsic ferroelectric behavior, offering an added dimension for advanced electronics and in-memory computing.[21,22] The device performance of indium selenide transistors degrades when exposed to atmospheric conditions due to chemical reactions with water and oxygen.[23] By encapsulating InSe transistor with indium, both the carrier mobility and stability of InSe are improved, providing a hopeful route for integrated circuit in the future.[24] Through hard shadow mask deposition, InSe transistor also shows enhanced performance against degradation.[25] Recently, it is reported that ballistic transport behavior in 2D InSe transistor can be realized by utilizing yttrium-doping-induced phase transition and resulting Ohmic contact.[26] InSe emerges as a promising candidate for optoelectronic applications, exhibiting enhanced photoresponsivity through vdW stacking

†Corresponding author. E-mail: hao@nju.edu.cn
‡Corresponding author. E-mail: sjliang@nju.edu.cn
§Corresponding author. E-mail: miao@nju.edu.cn

© 2024 Chinese Physical Society and IOP Publishing Ltd

with graphene, owing to efficient charge transport.[23,27,28] However, the interface between dielectric materials and 2D semiconductors typically hosts diverse carrier scattering centers and charge traps, significantly impacting InSe transistor electrical performance.[29,30] Consequently, achieving high-performance InSe transistors, characterized by attributes like high carrier mobility, on/off ratio, and on-state current density, remains a formidable challenge. There exists an urgent necessity to devise a comprehensive strategy to enhance its electrical characteristics.

In this work, we achieved improved electrical performance in few-layer InSe FETs by employing vdW stacking with h-BN and graphene to suppress dielectric-induced scattering and enhance the metal/semiconductor contacts. Initially, we constructed an InSe/BN vertical heterostructure to mitigate interface scattering originating from the SiO_2/Si substrate, which led to a notable enhancement in the electrical performance. Subsequently, by inserting graphene into InSe/BN heterostructure to enhance the contact behavior, the InSe FETs demonstrated improved electrical characteristics, including room-temperature carrier mobility exceeding 900 $cm^2 \cdot V^{-1} \cdot s^{-1}$, current on/off ratio $> 10^6$, and on-state current density of 1.1 mA/μm at $V_{ds} = 1$ V. Further theoretical calculations revealed that the improved electrical performances originate from evident charge transfer at the interface between InSe and graphene and preserved charge transport properties of InSe.

2. Materials and methods

2.1. Material characterizations

We performed optical microscopy (Nikon ECLIPSE Ci), and Raman/PL spectroscopy measurements (Witec 300R) under a 532.0 nm laser light. The spectra have been calibrated by the 520.7 cm^{-1} phonon mode of the silicon substrate. We also performed AFM characterizations (Bruker Multimode 8) of the mechanically exfoliated InSe, h-BN, and graphene.

2.2. Fabrication and measurement of devices

To prevent oxidation of InSe and ensure a clean heterostructure interface, the graphene, InSe, and h-BN microflakes were mechanically exfoliated onto the substrate in a glovebox filled with an inert atmosphere. The devices were fabricated by standard electron-beam lithography (FEI F50 with Raith pattern generation system) and electron-beam evaporation (5 nm Ti/45 nm Au). We measured the output and transfer curves of planar devices at room temperature by using an Agilent B1500A semiconductor analyzer connected to a probe station at room temperature. The temperature-dependent electrical measurements were performed in the Oxford cryostat with temperatures between 1.5 K and 300 K. The field-effect mobility of the device was calculated by fitting the linear region of the transfer curve with the following equation: $\mu = \frac{Ld}{wV_{ds}\varepsilon_0\varepsilon_r}\frac{dI_{ds}}{dV_{bg}}$, where L and w are the channel length and width, respectively, ε_0 (ε_r) is the vacuum (relative) permittivity, and d is the thickness of the SiO_2 layer (300 nm).

2.3. First-principles calculation

The electronic band structure and electron density difference of monolayer graphene, InSe, and graphene/InSe heterostructure were obtained by the CASTEP module based on density functional theory (DFT) on the platform of Materials Studio software. We applied a vacuum layer of 20 Å thickness along the Z-axis to avoid influence between the adjacent layers. The generalized gradient approximation (GGA) plane-wave pseudopotential method with the Perdew–Burke–Ernzerhof (PBE) functional was adopted for geometric optimization for the three structures. The Grimme DFT-D2 method was employed to consider the weak vdW interactions. For geometry optimization, charge density difference, and electrostatic potential calculations, the convergence criteria of the total energy change, the maximum force, stress, and displacement in this work were less than 5×10^{-6} eV/atom, 0.01 eV/Å, 0.02 GPa, and 5×10^{-4} Å, respectively. A Γ-centered $5\times5\times1$ Monkhorst–Pack k-point mesh was used for Brillion zone sampling. The energy cutoffs of the plane wave basis were set to 400 eV and 1200 eV for PBE and HSE06 functionals, respectively. The SCF tolerance was set to be 1×10^{-6} eV/atom. To ensure the accuracy of the calculated band structures, hybrid HSE06 functional was adopted due to underestimation of PBE functional to the band structure.

3. Results and discussion

We start by introducing atomic structure and material characterizations of γ-phase InSe, which belongs to the $R3m$ non-centrosymmetric space group with lattice parameters $a = b = 4.05$ Å, as shown in Fig. 1(a).[16,31] Furthermore, we performed Raman characterization to verify its crystallinity. Raman spectra (Fig. 1(b)) show three prominent peaks located at 116.6 cm^{-1}, 178.9 cm^{-1}, and 228.0 cm^{-1}, which are assigned to the characteristic modes of γ-phase InSe, in agreement with previous literature.[32,33] Moreover, the obvious PL characterisic peaks (see Fig. S2) are also assigned to InSe, indicating its high crystalline. To improve the electrical performances of InSe-based FETs, we fabricated transistors with mechanical exfoliated few-layer InSe on h-BN substrates since h-BN possesses an atomically flat surface and thus is widely used as a substrate for 2D transistors.[34] The output characteristic of InSe on h-BN shows linear I_{ds}–V_{ds} characteristics (Fig. 1(c)), suggesting the formation of ideal contact. Moreover, its source–drain currents can be well modulated by back-gate voltages, indicating its semiconducting behaviors. The transfer characteristic curves of InSe on h-BN

(Fig. 1(d)) indicate typical n-type transport behaviors, which is consistent with previous reports.[17,35] The carrier mobilities are estimated from the transfer characteristic curves to be 931 $cm^2 \cdot V^{-1} \cdot s^{-1}$. From the logarithm-type curves, the current on/off ratio for the InSe transistor at room temperature reaches 10^7. We undoubtedly ascribe the improvement of electrical performances of InSe transistors to the decrease of scattering effects induced by a dielectric layer h-BN.[34]

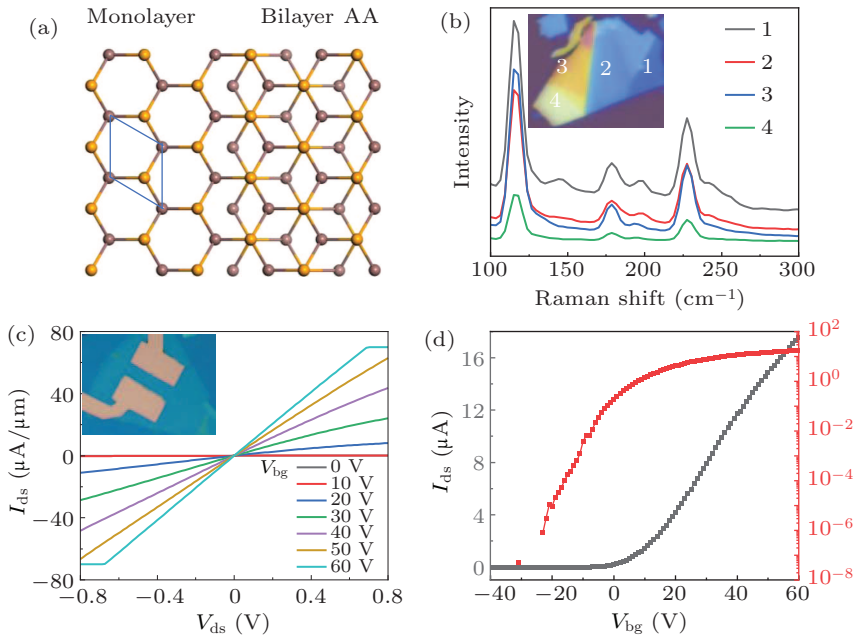


Fig. 1. (a) Top view of the atomical structure of monolayer (left region) and AA bernal stacking bilayer (right region) InSe. (b) Raman spectra taken from various sections of inserted optical microscopy image, respectively, demonstrate the high quality of the as-prepared InSe crystals. The back-gate voltages-dependent output characteristic curves (c), and transfer characteristic curves (d) in linear and logarithm scales for InSe FETs on h-BN substrate, respectively.

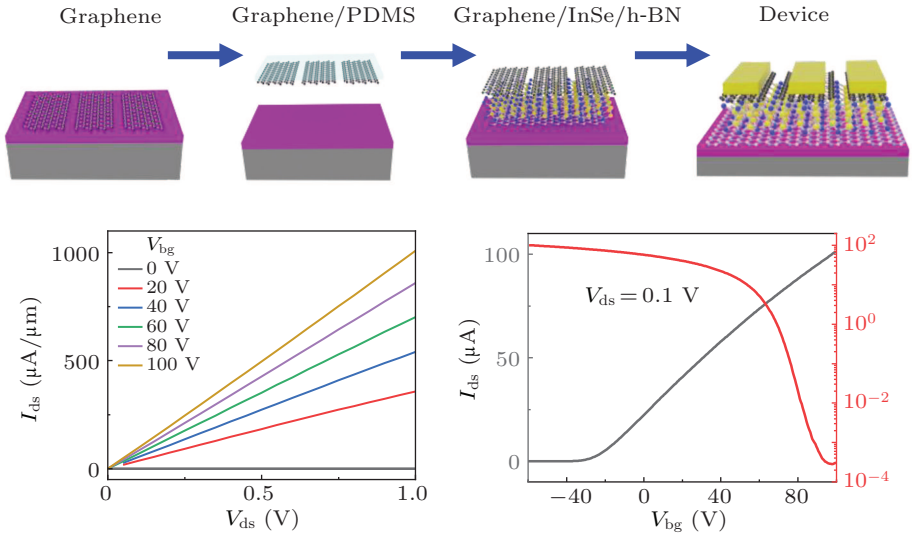


Fig. 2. (a) The schematic fabrication processes of graphene/InSe/h-BN vdW heterostructure and corresponding device structure, in which graphene serves as electrodes to improve the metal/semiconductor contact while h-BN can effectively decrease scattering effect from dielectric layer. (b), (c) The output and transfer characteristic curves of graphene/InSe/h-BN heterostructure-based transistors, respectively.

We further investigated the electrical performance improvement within InSe transistors by inserting graphene between metallic electrodes and InSe. Since graphene possesses ultrahigh conductivity and a dangling-free surface, it is expected to achieve enhanced metal/semiconductor contact by utilizing graphene as electrodes. First, we achieved graphene ribbons through the mechanically exfoliated method, as shown in Fig. 2(a). Then, we transferred the graphene ribbons onto the InSe/h-BN heterostructure using the PDMS-assisted dry transfer method. Finally, graphene/InSe/h-BN heterostructure-based transistors were fabricated by depositing metal electrodes on graphene. We also investigated the thicknesses of InSe, h-BN, and graphene before stacking together, as shown in Fig. S1. We can see that the thicknesses of InSe, h-BN, and graphene are around 15 nm, 10 nm, and 1 nm, respectively. The output characteristic curves (Fig. 2(b)) show linear I_{ds}–V_{ds} curves dependent on back-gate voltages, indicating Ohmic contact. Given the transfer characteristic

curves in Fig. 2(c), the current on/off ratio is $> 10^6$. Interestingly, the room-temperature carrier mobility reaches as high as 903 $cm^2 \cdot V^{-1} \cdot s^{-1}$, which is one of the highest values for 2D materials.[35] As a comparison, the mobility we obtained is much higher than that of molybdenum disulfide and equal to that of black phosphorus.[30,36] It is noteworthy that its on-state current density can reach 1.1 mA/μm, which is comparable to the value required for practical applications. Such enhancement of electrical performances can be attributed to the drastically improved semiconductor–metal contact by the use of graphene.

Given that theoretical results predict a smaller effective mass of InSe in the out-of-plane direction, it is expected to achieve ultrahigh electrical performances.[37] Therefore, we further designed an InSe/graphene-based vertical electrical device to investigate its transport behaviors in the out-of-plane direction, as shown in Fig. 3(a). From the output characteristic curves (Fig. 3(b)), one can see that the device shows perfect Ohmic contact, ascribed to graphene resulting in perfect metal/semiconductor contacts. Moreover, the source–drain currents show a gradual increase with rising temperatures. This behavior aligns with typical semiconductor characteristics, where higher temperatures boost carrier generation and mobility, affirming InSe's intrinsic semiconductor traits.[17,38] Interestingly, the Dirac point of graphene exhibited bipolar transport behavior near zero gate voltage, notably pronounced at room temperature (Fig. 3(c)). As the temperature decreased, this bipolar behavior gradually faded, indicating a shift in dominance towards InSe for transport characteristics at lower temperatures. This transition highlights the temperature-dependent interplay between graphene and InSe, where graphene's behavior diminishes as InSe governs transport properties at lower temperatures.[39] These findings provide further proof that the electrical conductivity of InSe matches that of graphene at lower temperatures, showcasing the theoretically predicted ultrahigh electrical conductivity of InSe.[37]

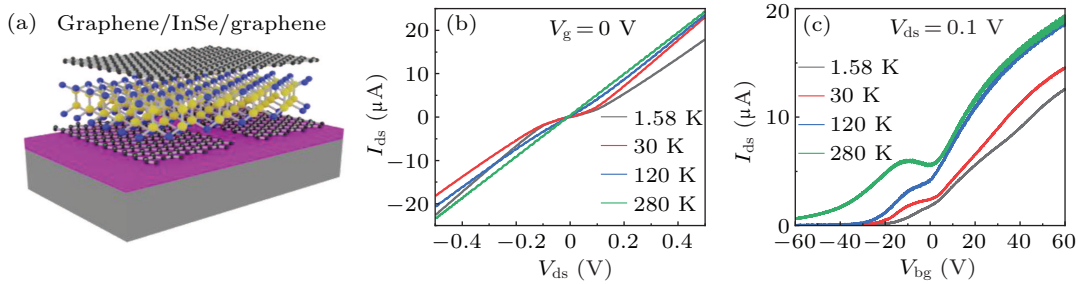


Fig. 3. (a) The schematic vertical device structure of graphene/InSe/graphene heterostructure. (b), (c) The temperature-dependent output and transfer characteristic curves for the graphene/InSe/graphene vertical transistor, respectively, in which both top and bottom electrodes are graphene.

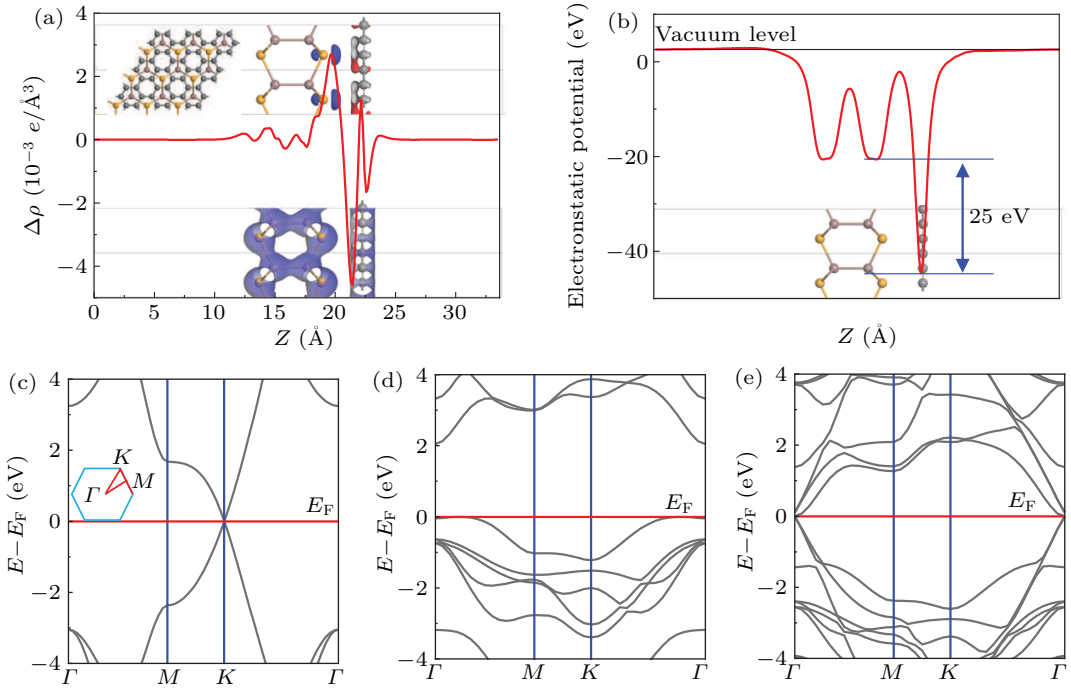


Fig. 4. (a) The electron density difference plot for graphene/InSe heterostructure. The upper illustration is the corresponding electron difference isosurface, in which red and blue regions denote electron accumulation and depletion, respectively. The inserted bottom illustrations are top and side views of InSe/graphene heterostructure. (b) Electrostatic potential along the z direction and corresponding atomic structure for graphene/InSe heterostructure (inset). (c)–(e) Band structures for monolayer graphene, InSe, and graphene/InSe heterostructure. The high-symmetry path of the three structures is Γ–M–K–Γ as shown in the inserted illustration in (c).

To unveil the mechanism of graphene-assisted electrical performance enhancement for InSe FETs, we further performed theoretical calculations of graphene/InSe heterostructure based on DFT theory. The interlayer distance between graphene and InSe is ~ 3.5 Å after full structural relaxation, in agreement with previous works.[40,41] We calculated the charge density difference (CDD) for graphene/InSe heterostructure according to the following equation: $\Delta\rho = \rho(\text{graphene/InSe}) - \rho(\text{graphene}) - \rho(\text{InSe})$, where ρ(graphene/InSe), ρ(graphene), ρ(InSe) represent the electron densities of graphene/InSe, graphene, and InSe, respectively. The contrast between CDD and electron density in the inserted figures demonstrates the charge reconstruction at the interface between graphene and InSe, as shown in Fig. 4(a). In detail, electrons are depleted from InSe and accumulated in the graphene layer, indicating effective charge transfer between graphene and InSe.[30] The electrostatic potential along the z direction (Fig. 4(b)) presents a large potential drop of around ~ 25 eV between graphene and InSe, indicating a large charge transfer at the interface.[40] In addition, the band structure for graphene (Fig. 4(c)) shows representative linear energy dispersion at the K point. As shown in Fig. 4(d), monolayer InSe exhibits an indirect bandgap with a gap of 2.0 eV forming between the conduction band minimum (CBM) at the Γ point and the valence band maximum (VBM) at Γ to M point, which is similar to previous literature.[41] The projected band structure for InSe/graphene heterostructure (Fig. 4(e)) seems to be a sum of isolated graphene and InSe and thus suggests that the transport behaviors of InSe are well preserved, which agrees with previous results.[42] These results jointly demonstrate that graphene is a promising candidate for high-efficiency charge injection in the InSe-based FETs.

4. Conclusion

In summary, we have systemically investigated improvement strategies of electrical performances for InSe-based FETs by interface engineering and achieved a high carrier mobility of 903 $\text{cm}^2\cdot\text{V}^{-1}\cdot\text{s}^{-1}$ at room temperature, current on/off ratio of 10^6, and current density of 1.1 mA/μm at $V_{\text{ds}} = 1$ V. It is demonstrated that graphene serves as the buffer layer to enhance the semiconductor–metal contact while h-BN effectively suppresses the dielectric layer-induced scattering effects. Theoretical calculations also unveil that graphene weakly interacts with InSe, which ensures the intrinsically ultrahigh carrier mobility of InSe. This work provides a general route towards high-performance electronics based on 2D vdW heterostructures.

Acknowledgements

Song Hao thanks the support of the National Natural Science Foundation of China (Grant No. 62204030). This work was supported in part by the National Natural Science Foundation of China (Grant Nos. 62122036, 62034004, 61921005, 61974176, and 12074176) and the Strategic Priority Research Program of the Chinese Academy of Sciences (Grant No. XDB44000000)

References

[1] Zhou J, Zhu C, Zhou Y, Dong J, Li P, Zhang Z, Wang Z, Lin Y C, Shi J, Zhang R, Zheng Y, Yu H, Tang B, Liu F, Wang L, Liu L, Liu G B, Hu W, Gao Y, Yang H, Gao W, Lu L, Wang Y, Suenaga K, Liu G, Ding F, Yao Y and Liu Z 2023 *Nat. Mater.* **22** 450
[2] Chang C, Chen W, Chen Y, Chen Y, Chen Y, Ding F, Fan C, Fan H J, Fan Z and Gong C 2021 *Acta Phys. Chim. Sin.* **37** 2108017
[3] Shin J, Kim H, Sundaram S, Jeong J, Park B I, Chang C S, Choi J, Kim T, Saravanapavanantham M, Lu K, Kim S, Suh J M, Kim K S, Song M K, Liu Y, Qiao K, Kim J H, Kim Y, Kang J H, Kim J, Lee D, Lee J, Kim J S, Lee H E, Yeon H, Kum H S, Bae S H, Bulovic V, Yu K J, Lee K, Chung K, Hong Y J, Ougazzaden A and Kim J 2023 *Nature* **614** 81
[4] Lu G, Yu K, Wen Z and Chen J 2013 *Nanoscale* **5** 1353
[5] Zhou S Y, Gweon G H, Fedorov A V, First P N, de Heer W A, Lee D H, Guinea F, Castro Neto A H and Lanzara A 2007 *Nat. Mater.* **6** 770
[6] Zhou Z, Hou F, Huang X, Wang G, Fu Z, Liu W, Yuan G, Xi X, Xu J, Lin J and Gao L 2023 *Nature* **621** 499
[7] Zhang K, She Y, Cai X, Zhao M, Liu Z, Ding C, Zhang L, Zhou W, Ma J, Liu H, Li L J, Luo Z and Huang S 2023 *Nat. Nanotechnol.* **18** 448
[8] Fu J H, Min J, Chang C K, Tseng C C, Wang Q, Sugisaki H, Li C, Chang Y M, Alnami I, Syong W R, Lin C, Fang F, Zhao L, Lo T H, Lai C S, Chiu W S, Jian Z S, Chang W H, Lu Y J, Shih K, Li L J, Wan Y, Shi Y and Tung V 2023 *Nat. Nanotechnol.* **18** 1289
[9] Liu Y, Liu S, Wang Z, Li B, Watanabe K, Taniguchi T, Yoo W J and Hone J 2022 *Nat. Electron.* **5** 579
[10] Daus A, Vaziri S, Chen V, Köroğlu Ç, Grady R W, Bailey C S, Lee H R, Schauble K, Brenner K and Pop E 2021 *Nat. Electron.* **4** 495
[11] Montblanch A R P, Barbone M, Aharonovich I, Atatüre M and Ferrari A C 2023 *Nat. Nanotechnol.* **18** 555
[12] Li L, Yang F, Ye G J, Zhang Z, Zhu Z, Lou W, Zhou X, Li L, Watanabe K, Taniguchi T, Chang K, Wang Y, Chen X H and Zhang Y 2016 *Nat. Nanotechnol.* **11** 593
[13] Doganov R A, O'Farrell E C T, Koenig S P, Yeo Y, Ziletti A, Carvalho A, Campbell D K, Coker D F, Watanabe K, Taniguchi T, Neto A H C and Özyilmaz B 2015 *Nat. Commun.* **6** 6647
[14] Island J O, Steele G A, van der Zant H S and Castellanos-Gomez A 2015 *2D Mater.* **2** 011002
[15] Wood J D, Wells S A, Jariwala D, Chen K S, Cho E, Sangwan V K, Liu X, Lauhon L J, Marks T J and Hersam M C 2014 *Nano Lett.* **14** 6964
[16] Bandurin D A, Tyurnina A V, Yu G L, Mishchenko A, Zólyomi V, Morozov S V, Kumar R K, Gorbachev R V, Kudrynskyi Z R, Pezzini S, Kovalyuk Z D, Zeitler U, Novoselov K S, Patanè A, Eaves L, Grigorieva I V, Fal'ko V I, Geim A K and Cao Y 2017 *Nat. Nanotechnol.* **12** 223
[17] Sucharitakul S, Goble N J, Kumar U R, Sankar R, Bogorad Z A, Chou F C, Chen Y T and Gao X P A 2015 *Nano Lett.* **15** 3815
[18] Li W B and Giustino F 2020 *Phys. Rev. B* **101** 035201
[19] Kress-Rogers E, Nicholas R J, Portal J C and Chevy A 1982 *Solid State Commun.* **44** 379
[20] Gao A, Lai J, Wang Y, Zhu Z, Zeng J, Yu G, Wang N, Chen W, Cao T, Hu W, Sun D, Chen X, Miao F, Shi Y and Wang X 2019 *Nat. Nanotechnol.* **14** 217
[21] Sui F, Jin M, Zhang Y, Qi R, Wu Y N, Huang R, Yue F and Chu J 2023 *Nat. Commun.* **14** 36
[22] Liao J, Wen W, Wu J, Zhou Y, Hussain S, Hu H, Li J, Liaqat A, Zhu H, Jiao L, Zheng Q and Xie L 2023 *ACS Nano* **17** 6095
[23] Hao S, Yan S, Wang Y, Xu T, Zhang H, Cong X, Li L, Liu X, Cao T, Gao A, Zhang L, Jia L, Long M, Hu W, Wang X, Tan P, Sun L, Cui X, Liang S J and Miao F 2020 *Small* **16** 1905902

[24] Li M, Lin C Y, Yang S H, Chang Y M, Chang J K, Yang F S, Zhong C, Jian W B, Lien C H, Ho C H, Liu H J, Huang R, Li W, Lin Y F and Chu J 2018 *Adv. Mater.* **30** 1803690

[25] Zhang Y, Sun X, Jia K, Yin H, Luo K, Yu J and Wu Z 2021 *Nanomaterials* **11** 3311

[26] Jiang J, Xu L, Qiu C and Peng L M 2023 *Nature* **616** 470

[27] Chen Z, Biscaras J and Shukla A 2015 *Nanoscale* **7** 5981

[28] Lei S, Ge L, Najmaei S, George A, Kappera R, Lou J, Chhowalla M, Yamaguchi H, Gupta G, Vajtai R, Mohite A D and Ajayan P M 2014 *ACS Nano* **8** 1263

[29] Feng W, Zheng W, Cao W and Hu P 2014 *Adv. Mater.* **26** 6587

[30] Li W, Gong X, Yu Z, Ma L, Sun W, Gao S, Köroğlu Ç, Wang W, Liu L, Li T, Ning H, Fan D, Xu Y, Tu X, Xu T, Sun L, Wang W, Lu J, Ni Z, Li J, Duan X, Wang P, Nie Y, Qiu H, Shi Y, Pop E, Wang J and Wang X 2023 *Nature* **613** 274

[31] Hamer M J, Zultak J, Tyurnina A V, Zólyomi V, Terry D, Barinov A, Garner A, Donoghue J, Rooney A P, Kandyba V, Giampietri A, Graham A, Teutsch N, Xia X, Koperski M, Haigh S J, Fal'ko V I, Gorbachev R V and Wilson N R 2019 *ACS Nano* **13** 2136

[32] Zheng T, Wu Z, Nan H, Yu Y, Zafar A, Yan Z, Lu J and Ni Z 2017 *RSC Adv.* **7** 54964

[33] Dean C R, Young A F, Meric I, Lee C, Wang L, Sorgenfrei S, Watanabe K, Taniguchi T, Kim P, Shepard K L and Hone J 2010 *Nat. Nanotechnol.* **5** 722

[34] Sun Y J, Pang S M and Zhang J 2022 *J. Phys. Chem. Lett.* **13** 3691

[35] Ho P H, Chang Y R, Chu Y C, Li M K, Tsai C A, Wang W H, Ho C H, Chen C W and Chiu P W 2017 *ACS Nano* **11** 7362

[36] Li T, Guo W, Ma L, Li W, Yu Z, Han Z, Gao S, Liu L, Fan D, Wang Z, Yang Y, Lin W, Luo Z, Chen X, Dai N, Tu X, Pan D, Yao Y, Wang P, Nie Y, Wang J, Shi Y and Wang X 2021 *Nat. Nanotechnol.* **16** 1201

[37] Li W and Giustino F 2020 *Phys. Rev. B* **101** 035201

[38] Wasala M, Patil P D, Ghosh S, Alkhaldi R, Weber L, Lei S, Vajtai R, Ajayan P M and Talapatra S 2020 *2D Mater.* **7** 025030

[39] Novoselov K S, Geim A K, Morozov S V, Jiang D, Zhang Y, Dubonos S V, Grigorieva I V and Firsov A A 2004 *Science* **306** 666

[40] Yao X and Zhang X 2021 *ACS Omega* **6** 13426

[41] Narin P, All Abbas J M, Kutlu-Narin E, Lisesivdin S B and Ozbay E 2023 *Comput. Mater. Sci.* **222** 112114

[42] Pham K D, Hieu N N, Ilyasov V V, Phuc H V, Hoi B D, Feddi E, Thuan N V and Nguyen C V 2018 *Superlattices Microstruct.* **122** 570